23rd International Conference on Material Forming (ESAFORM 2020)

Reduced-Integrated 8-Node Hexahedral Solid-Shell Element for the Macroscopic Forming Simulation of Continuous Fibre-Reinforced Polymers

Bastian Schäfer[a],*, Dominik Dörr[a,b], Luise Kärger[a]

[a]Karlsruhe Institute of Technology (KIT), Institute of Vehicle System Technology (FAST), 76131 Karlsruhe, Germany
[b]SIMUTENCE GmbH, 76131 Karlsruhe, Germany

* Corresponding author. Tel.: +49-721-608-41821; fax: +49-721-608-945905. E-mail address: bastian.schaefer@kit.edu

Abstract

Finite element (FE) forming simulation offers the possibility of a detailed analysis of the deformation behaviour of continuously fibre-reinforced polymers (CFRPs) during forming, in order to predict possible manufacturing effects such as wrinkling or local changes in fibre volume content. The majority of macroscopic simulations are based on conventional two-dimensional shell elements with large aspect ratios to model the membrane and bending behaviour of thin fibrous reinforcements efficiently. However, without a three-dimensional element approach, stresses and strains in thickness direction cannot be modelled accurately. Commercially available linear 3D solid elements for this purpose are rarely suitable for forming simulations since they are subjected to several locking phenomena under bending deformation, especially with large aspect ratios. To alleviate this problem, so-called solid-shell elements based on the assumed natural strain (ANS) and enhanced assumed strain (EAS) method can be used. Therefore, a locking-free explicit reduced-integrated 8-node-hexahedron solid-shell element, based on the initial work of Schwarze and Reese (2011), is implemented in the commercially available FE solver Abaqus. Its suitability for macroscopic modelling of the forming behaviour of fibrous reinforcements is outlined in this work. The presented element combines the advantages of a locking-free out-of-plane deformation behaviour of conventional thin shell elements with the advantage of maintaining a fully three-dimensional material model and geometry description.

Keywords: Solid-Shell; Forming; Process Simulation; Finite Element Analysis (FEA)

1. Introduction

Finite element (FE) forming simulations can be used to analyse the manufacturing process of continuously fibre-reinforced polymers (CFRPs) and predict effects like fibre reorientation or wrinkling. Therefore, state of the art forming simulation approaches mainly apply conventional two-dimensional shell approaches [1] to model the deformation of thin fibrous reinforcements, since they allow for high aspect ratios, while still accurately describing the membrane and bending behaviour. However, those approaches cannot model out-of-plane compaction, which is an important forming

mechanism to predict local fibre volume contents [2] and influences the permeability of the reinforcement during manufacturing processes such as wet compressions moulding [3]. To predict these effects and the final thickness of the part, a three-dimensional FE-formulation is necessary.

The problem with the application of common solid elements for composite forming simulations is the occurrence of numerical locking phenomena, which cause a too high bending stiffness especially for elements with high aspect ratios [4]. An approach to alleviate this problem are so-called solid-shell elements. These elements combine techniques like reduced integration and modifications of the strain field to eliminate

geometrical and material locking phenomena [5]. However, only little research is focused on the application of solid-shell elements for metal forming [6-8] and especially composite forming [9].

The hexahedral solid-shell element proposed by Schwarze and Reese [10, 11] and extended to an explicit formulation by Pagani et. al. [12] is used in this work. The element is developed for large deformations and is based on a reduced in-plane integration, with an arbitrary number of integration points over the thickness together with a suitable hourglass stabilization. The key features in the element formulation to eliminate locking phenomena are the assumed natural strain (ANS) and enhanced assumed strain (EAS) method to improve the accuracy for thin shell problems. Furthermore, Taylor expansions of the Green-Lagrange strain and second Piola-Kirchhoff stress along the thickness direction are carried out to improve the numerical efficiency. The element was chosen to be evaluated for an application in composite forming, due to its already successful application in large deformation analysis of composite materials [13], but without contact boundary conditions, and sheet metal forming [6]. Additionally, Robertsson et. al. [8] have demonstrated the good expandability of the element formulation for different materials by extending it for packaging forming simulations of anisotropic paperboard models.

In comparison, the solid-shell element proposed by Flores [7] applies similar techniques to eliminate locking phenomena for the element's top and bottom surface individually and an additional assumed strain approximation for the in-plane strains. Flores directly compares the element's behaviour for different examples with the work of Schwarze and Reese [11] achieving similar results. However, it requires the additional tuning of hourglass stabilization parameters.

The most advanced solid-shell element for composite forming of thermoplastic prepreg was proposed by Xiong et. al. [9] and is a 6-node prismatic element based on a DKT ("Discrete Kirchhoff Theory") formulation. However, it requires an additional global degree of freedom in the element centre to avoid thickness locking, in contrast to an internal degree of freedom based on the EAS method [12].

In this work, initial steps towards an 8-node hexahedral solid-shell element suitable for the macroscopic forming simulation of thin fibrous reinforcements are presented. For this purpose, the selected element formulation is utilized within a FE-User-Element (VUEL) in ABAQUS/EXPLICIT. To ensure a computationally efficient implementation, a MATHEMATICA-based programming environment called ACEGEN [14] is used. ACEGEN provides a symbolic implementation and differentiation combined with a simultaneous runtime-optimization.

In the following, the main aspects of the element formulation are presented. The locking-free bending behaviour of the selected element for high aspect ratios, large deformations and low stiffness is shown by a comparison with conventional shell and commercially available solid element formulations in a cantilever-bending scenario. Finally, the solid-shell element is applied to forming simulation of a generic geometry, and its suitability for macroscopic forming simulation is evaluated.

Nomenclature – Solid-Shell element

$\hat{\bullet}$	Tensor in Voigt notation
$\bar{\bullet}$	Tensor in isoparametric coordinates
$\bullet^{\text{dev}}$	Deviatoric part of a tensor
$\bullet_c$	Compatible part of a tensor
$\bullet_e$	Enhanced part of a tensor
$\bullet^*$	Quantity related to out-of-plane integration
$\bullet^{\text{hg}}$	Quantity related to hourglass stabilization
a	Aspect ratio
g_{ext}	Virtual work of external loading
J^0	Jacobian determinant at the element centre
w_e	Enhanced degree of freedom
$\mu_{\text{eff}}^{\text{hg}}$	Effective shear modulus
$\{\xi, \eta, \zeta\}$	Isoparametric coordinates
$\boldsymbol{u}$	Displacement vector
$\boldsymbol{\xi}^*$	Normal through the element centre
$\boldsymbol{E}$	Total Green-Lagrange strain tensor
$\boldsymbol{S}$	Second Piola-Kirchhoff stress tensor

2. Solid-Shell element

As mentioned above the solid-shell element originally proposed by Schwarze and Reese [10] was chosen for the study in this work. It is derived from the standard isoparametric 8-node hexahedral brick-element with tri-linear shape functions and is based on the two-field variational functionals [15]

$$g_1(\boldsymbol{u}, \boldsymbol{E}_e) = \int_{V_0} (S(E) \cdot \delta \boldsymbol{E}_c + \rho_0 \ddot{\boldsymbol{u}} \cdot \delta \boldsymbol{u}) dV + g_{ext} = 0 \quad (1)$$

$$g_2(\boldsymbol{u}, \boldsymbol{E}_e) = \int_{V_0} S(E) \cdot \delta \boldsymbol{E}_e \, dV = 0, \quad (2)$$

where g_{ext} denotes the virtual work of external loading and $S(E)$ the second Piola-Kirchhoff stress tensor. According to the EAS concept, the Green-Lagrange strain tensor $\boldsymbol{E}$ is additively split $\boldsymbol{E} = \boldsymbol{E}_c + \boldsymbol{E}_e$, into a compatible part $\boldsymbol{E}_c(\boldsymbol{u})$, depending solely on the displacement vector $\boldsymbol{u}$, and an enhanced part $\boldsymbol{E}_e(w_e)$, depending on a single additional enhanced degree of freedom w_e, leading to the second variational functional, cf. Equation 2.

The element uses a reduced in-plane integration and a full integration (at least 2 integration points) in thickness direction. This results in all integration points being located on the normal through the centre of the element, defined in isoparametric coordinates ($\xi_1 = \xi$, $\xi_2 = \eta$ and $\xi_3 = \zeta$) by $\boldsymbol{\xi}^* = \{0, 0, \zeta\}^\top$, as illustrated in Figure 1 (a). This integration scheme was demonstrated to be computationally efficient and suitable for explicit dynamics simulation by Pagani et al. [12]. Additionally, it captures nonlinearities in the thickness direction for thin structures very well, compared to commercially available explicit reduced-integration elements that mostly use a single integration point in the element centre.
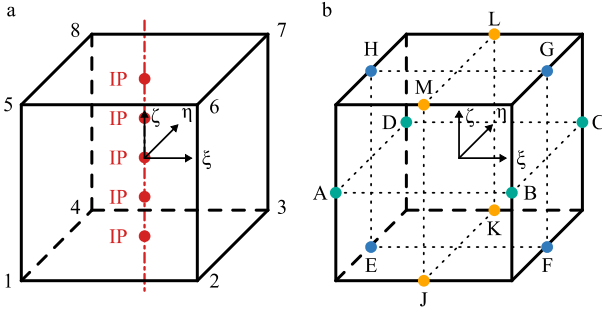
Fig. 1. Isoparametric solid-shell element | (a) Element nodes 1-8 and integration points IP, (b) Sampling points for the ANS method

The ANS method is adopted for the compatible strains in the isoparametric domain $\bar{E}_c$. The strain components prone to locking phenomena are evaluated at specific sample points along the element edges at which the respective locking does not occur, cf. Figure 1 (b), and interpolated by means of bi-linear shape functions. This is used for the transverse normal components $\bar{E}_{c\zeta\zeta}$ (sample points $I_1 = A, B, C, D$) to eliminate curvature-thickness locking, as proposed by Betsch and Stein [16], and for the transverse shear components $\bar{E}_{c\eta\zeta}$ and $\bar{E}_{c\xi\zeta}$ (sample points $I_2 = E, F, G, H$ and $I_3 = J, K, L, M$ respectively) to alleviate transverse-shear locking, as first proposed for shell elements by Bathe and Dvorkin [17]. These modifications result in:

$$\bar{E}_{c\zeta\zeta}^{ANS} = \sum_{I_1=A}^{D} \frac{1}{4}\left(1 + \xi_{I_1}\xi\right)\left(1 + \eta_{I_1}\eta\right)\bar{E}_{c\zeta\zeta}^{I_1}, \tag{3}$$

$$\bar{E}_{c\eta\zeta}^{ANS} = \sum_{I_2=E}^{H} \frac{1}{4}(1 + \xi_{I_2}\xi)(1 + \zeta_{I_2}\zeta)\bar{E}_{c\eta\zeta}^{I_2}, \tag{4}$$

$$\bar{E}_{c\xi\zeta}^{ANS} = \sum_{I_3=J}^{M} \frac{1}{4}(1 + \eta_{I_3}\eta)(1 + \zeta_{I_3}\zeta)\bar{E}_{c\xi\zeta}^{I_3}. \tag{5}$$

The ANS method results in constant transverse normal strain $\bar{E}_{c\zeta\zeta}^{ANS}$ in the out-of-plane-direction ζ, while the normal in-plane strains $\bar{E}_{c\xi\xi}$ and $\bar{E}_{c\eta\eta}$ remain linear with respect to their corresponding isoparametric coordinate ξ and η. Therefore, to avoid volumetric locking phenomena, the enhanced strain tensor $\bar{E}_e$ is constructed to extend $\bar{E}_{\zeta\zeta}$ by a linear component. This requires only a single enhanced degree of freedom, which results in Voigt notation ($\hat{\bullet}$) to:

$$\hat{\bar{E}}_e = \hat{\bar{B}}_e w_e \text{ with } \hat{\bar{B}}_e = \{0, 0, \zeta, 0, 0, 0\}^\top. \tag{6}$$

A main advantage of this simple formulation for $\hat{\bar{E}}_e$, as shown by Pagani et al. [12], is that w_e can be estimated within a single iteration of an explicit dynamic integration scheme, due to the small explicit time step size.

To further increase the numerical efficiency, a Taylor expansion of the compatible Green-Lagrange strain with respect to the element centre $\xi = 0$ is carried out

$$\hat{E}_c \approx \underbrace{\hat{E}_c^0 + \zeta\hat{E}_c^\zeta + \zeta^2\hat{E}_c^{\zeta\zeta}}_{\hat{E}_c^*}$$
$$+ \underbrace{\xi\hat{E}_c^\xi + \eta\hat{E}_c^\eta + \xi\eta\hat{E}_c^{\xi\eta} + \eta\zeta\hat{E}_c^{\eta\zeta} + \xi\zeta\hat{E}_c^{\xi\zeta}}_{\hat{E}_c^{hg}}, \tag{7}$$

where $\hat{E}_c^{(\bullet)}$ are constant tensors. The compatible Green-Lagrange strain is separated into a part related to the out-of-plane integration $\hat{E}_c^*$ and a part unaffected by the numerical integration $\hat{E}_c^{hg}$, which is essential to the hourglass stabilization of the reduced integration scheme.

Similar to Equation 7, a Taylor expansion of the second Piola-Kirchhoff stress along the out-of-plane direction ξ^* is carried out

$$\hat{S} \approx \underbrace{\hat{S}(E^*)}_{\hat{S}^*} + \underbrace{\frac{\partial \hat{S}}{\partial \hat{E}}\bigg|_{\xi=\xi^*}}_{\hat{C}^*}\left(\xi\hat{E}_c^\xi + \eta\hat{E}_c^\eta + \eta\zeta\hat{E}_c^{\eta\zeta} + \xi\zeta\hat{E}_c^{\xi\zeta}\right)$$
$$= \hat{S}^* + \hat{S}^{hg}, \tag{8}$$

where the stress tensor is separated into the parts related to out-of-plane integration $\hat{S}^*$ and hourglass stabilization $\hat{S}^{hg}$. The complexity of the hourglass stabilization part is reduced by replacing the material tangent $\hat{C}^*$ with a constant deviatoric matrix $\hat{C}^{hg} = \mu_{eff}^{hg}\hat{I}^{dev}$, defined by an effective shear modulus μ_{eff}^{hg} and the deviatoric part of the fourth-order identity tensor in Voigt notation $\hat{I}^{dev}$. This method results in a locking-free hourglass part of the stress and in combination with the constant tensors $\hat{E}_c^{(\bullet)}$, resulting from the Taylor approximation in Equation 7, allows for an analytical integration of the hourglass parts of Equation 1. Thereby, the effective shear modulus is adaptively calculated by

$$\mu_{eff}^{hg} = \sum_i \left(\frac{1}{2}\sqrt{\frac{S^{*dev} \cdot S^{*dev}}{E^{*dev} \cdot E^{*dev}}}\right)\bigg|_i \omega_i \tag{9}$$

where n_{IP} is the number of integration points and ω_i the respective weighting factors.

Finally, Equations 1 and 2 have to be discretized and solved on element level. Therefore, the infinitesimal volume element on element level is approximated by $dV^e \approx J^0 d\Omega^e$, where the Jacobian determinant is replaced by its value in the element centre $J^0 = J|_{\xi=\eta=\zeta=0}$. The discretized weak element formulation corresponding to Equation 1 and 2 can be approximated as follows:

$$G_1 = R_u^* + R_u^{hg} + M\ddot{u} - G_{ext} = 0 \text{ and } G_2 = 0, \tag{10}$$

with M being the element mass matrix and G_{ext} being the external element force vector. The internal forces related to the

out-of-plane integration $\boldsymbol{R}_u^*$, the hourglass stabilization $\boldsymbol{R}_u^{hg}$ and the enhanced part G_2 are derived as

$$\boldsymbol{R}_u^* = \int_{-1}^{1} \left(\widehat{\boldsymbol{B}}_c^0 + \zeta\widehat{\boldsymbol{B}}_c^\zeta + \zeta^2\widehat{\boldsymbol{B}}_c^{\zeta\zeta}\right)^\top \widehat{\boldsymbol{S}}^* d\zeta \, 4J^0 , \tag{11}$$

$$\begin{aligned} \boldsymbol{R}_u^{hg} = \frac{8}{3}&\left(\widehat{\boldsymbol{B}}_c^{\xi\top} \boldsymbol{C}^{hg} \boldsymbol{E}_c^\xi + \widehat{\boldsymbol{B}}_c^{\eta\top} \boldsymbol{C}^{hg} \boldsymbol{E}_c^\eta\right) J^0 \\ +\frac{8}{9}&\left(\widehat{\boldsymbol{B}}_c^{\xi\zeta\top} \boldsymbol{C}^{hg} \boldsymbol{E}_c^{\xi\zeta} + \widehat{\boldsymbol{B}}_c^{\eta\zeta\top} \boldsymbol{C}^{hg} \boldsymbol{E}_c^{\eta\zeta}\right) J^0 , \end{aligned} \tag{12}$$

$$G_2 = \int_{-1}^{1} \widehat{\boldsymbol{B}}_e^\top \widehat{\boldsymbol{S}}^* d\zeta \, 4J^0 , \tag{13}$$

where the $\widehat{\boldsymbol{B}}_c^{(\cdot)}$ matrices represent the relation between the respective strains $\widehat{\boldsymbol{E}}_c^{(\cdot)}$ and displacements $\boldsymbol{u}$, according to $\widehat{\boldsymbol{E}}_c^{(\cdot)} = \widehat{\boldsymbol{B}}_c^{(\cdot)}\boldsymbol{u}$.

The main advantages of the solid-shell element formulation above, is the possibility to use a fully three-dimensional constitutive law for the relation $\widehat{\boldsymbol{S}}^*$ (cf. Equation 8) and therefore describe the behaviour in thickness direction compared to conventional shell elements. Additionally, the locking-free deformation behaviour allows for a larger aspect ratio of the element and thus a reduction of the computational effort in forming simulations compared to commercially available solid elements.

3. Numerical studies

The formulation of the solid-shell element outlined above is implemented within a FE-User-Element (VUEL) in ABAQUS/EXPLICIT and verified by numerical case studies. In order to investigate the influence of a locking-free deformation behaviour on macroscopic forming simulations as isolated as possible, a simple elastic isotropic material behaviour is utilized.

In the following, the locking-free bending behaviour is presented by means of a comparison to conventional shell and commercially available solid elements in a cantilever-bending scenario. Subsequently, the forming behaviour is evaluated by comparing the simulation results of a hemisphere test.

3.1. Cantilever-bending test

The macroscopic forming behaviour of thin fibrous reinforcements is characterised by a high in-plane stiffness in fibre direction combined with a low bending stiffness. Since locking phenomena are mainly prevalent in bending dominated deformations, it is therefore necessary to have a completely locking-free element formulation in order to not overestimate the low bending stiffness of composite pre-products at processing conditions.

As a first example, the out-of-plane bending behaviour of a cantilever plate strip under a tip load is investigated. The plate strip, as illustrated in Figure 2, has a width of $w = 10$ mm, a length of $l = 60$ mm, a thickness of $t = 0.3$ mm, and a tip load of $F = 0.4$ mN is applied. A Young's modulus of $E =$

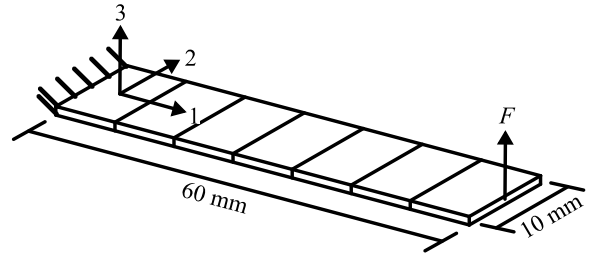100 MPa and Poisson ratio of $\nu = 0.3$ is chosen to test the bending behaviour for low stiffness.

Fig. 2. Cantilever plate strip | Geometry and load

The beam is discretized by only one element in thickness and width direction. The number of elements in length direction and therefore the element's aspect ratio $a = l_e/t$ is varied between $a \in \{2.5, 5, 10, 20, 40\}$ to study the convergence behaviour. The solid-shell element ($n_{IP} = 3$) is compared to in ABAQUS/EXPLICIT commercially available reduced integrated shell (S4R) and solid (C3D8R) elements, as well as a fully integrated solid element (C3D8) and a reduced integrated solid element with an enhanced hourglass stabilization (C3D8R-Enh). The C3D8R-Enh element introduces up to six additional internal degrees of freedom based on the EAS method, to augment the hourglass stabilization forces of the C3D8R element [18]. The results of this study for the tip displacement are shown in Figure 3.
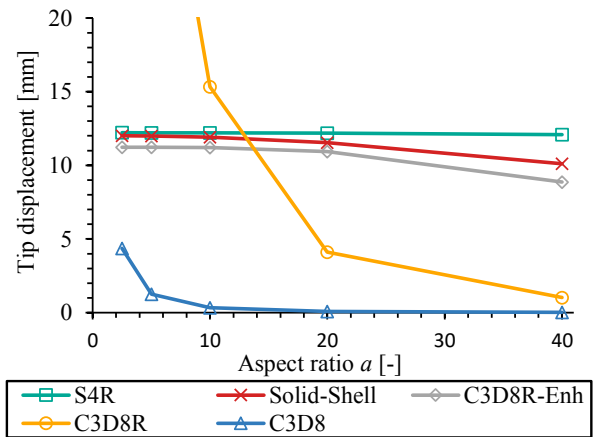

Fig. 3. Cantilever-bending test | Results for the conventional shell (S4R), solid-shell and different commercially available solid (C3D8, C3D8R and C3D8R-Enh) elements

As expected, the shell element achieves a converged solution already for very high aspect ratios and is used in this comparison as the desired reference solution, based on the assumption that it has a locking-free out-of-plane bending behaviour.

The C3D8-element behaves too stiff due to locking effects and even for an aspect ratio as low as 2.5 is unsuited for this bending problem. In comparison to the fully integrated solid, the reduced integrated solid element with only one integration point (C3D8R) achieves a slightly better solution for high

aspect ratios. However, for low aspect ratios a single element with only one integration point over the thickness is unable to model a pure bending deformation and as a result behaves completely compliant. Therefore, the reduced integrated solid element is subjected to locking phenomena for high aspect ratios and not suitable to model a pure bending behaviour for low aspect ratios.

The result of the C3D8R-Enh element is the best commercially available solid element for very high aspect ratios and it is able to model the cantilever-bending with results close to the reference solution for small aspect ratios, despite a reduced integration scheme with a single integration point.

The best results are achieved by the solid-shell element presented in Section 2. For an aspect ratio under $a \leq 10$ its tip displacement is close to the reference solution and converges towards the shell's solution for $a \leq 5$.

3.2. Hemisphere test

The influence of a locking-free element formulation on the macroscopic forming behaviour is investigated in a numerical study by means of a hemisphere test. A single layer with a thickness of $t = 0.3$ mm and the same material parameters as in Section 3.1 is used. An aspect ratio of $a = 10$ was chosen to reduce the computational effort, while still ensuring a nearly locking-free bending deformation for the solid-shell element, based on the results of Section 3.1.

Figure 4 shows the deformation during the forming simulation for a remaining tool stroke Δu of 7 mm, 3.5 mm and 0.0 mm for all elements investigated in Section 3.1. In agreement with the results of Boisse et al. [19], the bending behaviour has a significant influence on the distinct wrinkling pattern for the different element types.

Based on the assumptions and results of Section 3.1, again, the shell element (S4R) is used as the desired reference solution. During its forming simulation a very high number of small wrinkles are developed in all directions.

An increase in size and decrease of the number of wrinkles is observed for the fully integrated solid element (C3D8),

which shows a stiffer behaviour in the cantilever-bending test (cf. Figure 3). However, the general orientation of the onset of wrinkles is similar to the results of the shell element.

The deformation behaviour of the reduced integrated solid element (C3D8R) is completely different compared to all other examined elements. The orientation of the onset of wrinkles is only perpendicular to the edges of the thin sheet and they are perfectly straight compared to the rather irregular wrinkling pattern of the reference solution. This again indicates that a single layer of C3D8R elements with only one integration point in thickness direction is not suitable to model bending dominated problems.

The results of the solid element with enhanced hourglass stabilization (C3D8R-Enh) and of the solid-shell element are very similar to each other. For both element types, the locations as well as size of wrinkling is in good agreement with the reference shell element.

The hemisphere tests show that the element formulation and thus locking-free bending behaviour for larger aspect ratios has a significant influence on the macroscopic forming behaviour, even for a simple linear isotropic material model.

4. Conclusion and outlook

This work presents an initial study on a solid-shell element for the macroscopic forming simulation of thin fibrous reinforcements. Compared to a conventional shell element, the advantage of a three-dimensional element formulation is its capability to model strains in thickness direction and to predict, e.g., out-of-plane compaction. However, commercially available solid elements are prone to locking phenomena under bending deformation. Therefore, a solid-shell element formulation was selected from literature, and its main aspects relevant for a locking-free behaviour are highlighted. The effects of a locking-free behaviour were investigated in a numerical study, by comparison to conventional shell and commercially available solid elements. The advantage of solid-shell elements compared to commercially available solid elements in the modelling of bending dominated problems was
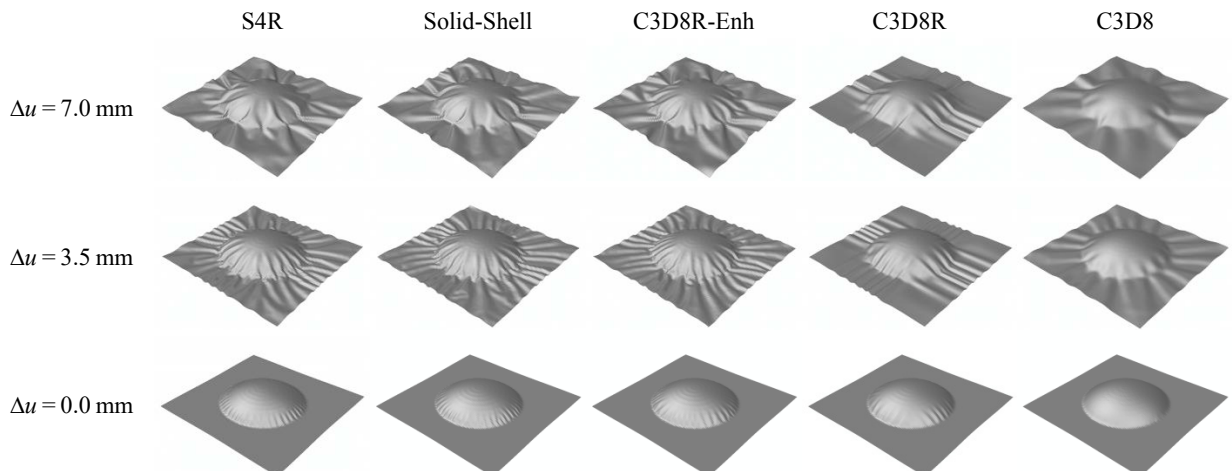

Fig. 4. Hemisphere test | Results for a remaining tool stroke Δu of 7.0 mm, 3.5 mm and 0.0 mm for the conventional shell (S4R), solid-shell and different commercially available solid (C3D8, C3D8R and C3D8R-Enh) elements

shown and the necessity of a suitable element formulation for macroscopic forming applications was demonstrated.

The solid-shell element analysed in this work is shown to be suitable to model the deformation behaviour of high aspect ratios with a prediction accuracy comparable to conventional shell elements. This locking-free behaviour is a necessary prerequisite to model the deformation of thin fibrous reinforcements efficiently. However, the results were only shown for a simple linear elastic material model and need to be re-evaluated for a highly anisotropic material behaviour more comparable to fibrous reinforcements, which will be a scope of future investigations.

Additionally, like standard shell approaches the presented element formulation cannot be applied directly to fibrous reinforcements, which require a decoupling of the membrane and bending behaviour due to their high tensile stiffness in fibre direction and comparably low bending stiffness [20]. This requirement was one of the reasons for the decision to implement a FE-User-Element based on the selected element formulation, rather than applying a commercially available solid element. As shown in Section 3, there are solid elements (C3D8R-Enh) commercially available, which are similarly suited for bending dominated problems as the presented solid-shell element. However, since the C3D8R-Enh element has only one single integration point and performs well in bending scenarios purely because of the enhanced hourglass parts of the stress, a decoupling of the membrane and bending behaviour would not be possible within this single element.

In comparison, the presented solid-shell element is locking-free in all parts of the stress and utilizes a variable number of integration points in thickness direction. These features in combination with the already performed Taylor expansion in thickness direction should allow for a decoupling of the bending and membrane behaviour within a single element. This will be the main focus of future work in order to meet the prerequisites for a macroscopic forming simulation of thin fibrous reinforcements.

Furthermore, the benefits of modelling the thickness direction will be investigated in the context of composite forming. Since state of the art forming approaches are mainly based on shell elements and therefore often limited in the consideration of the out-of-plane behaviour. The utilization of a fully three-dimensional approach should enable a better approximation of forming effects like local thickness changes and fibre volume content [2], by investigating the compaction behaviour.

Acknowledgements

References

[1] Bussetta P, Correia N. Numerical forming of continuous fibre reinforced composite material: A review. Composites Part A: Applied Science and Manufacturing 2018;113:12–31.

[2] Galkin S, Kunze E, Kärger L, Böhm R, Gude M. Experimental and Numerical Determination of the Local Fiber Volume Content of Unidirectional Non-Crimp Fabrics with Forming Effects. J. Compos. Sci. 2019;3(1):19.

[3] Poppe C, Rosenkranz T, Dörr D, Kärger L. Comparative experimental and numerical analysis of bending behaviour of dry and low viscous infiltrated woven fabrics. Composites Part A: Applied Science and Manufacturing 2019;124:105466.

[4] Belytschko T. Nonlinear finite elements for continua and structures. 2nd ed. Chichester: Wiley; 2014.

[5] Hauptmann R, Schweizerhof K. A systematic development of 'solid-shell' element formulations for linear and non-linear analyses employing only displacement degrees of freedom. Int. J. Numer. Meth. Engng. 1998;42(1):49–69.

[6] Schwarze M, Vladimirov IN, Reese S. Sheet metal forming and springback simulation by means of a new reduced integration solid-shell finite element technology. Computer Methods In Applied Mechanics And Engineering 2011;200(5-8):454–76.

[7] Flores FG. A simple reduced integration hexahedral solid-shell element for large strains. Computer Methods In Applied Mechanics And Engineering 2016;303:260–87.

[8] Robertsson K, Borgqvist E, Wallin M, Ristinmaa M, Tryding J, Giampieri A et al. Efficient and accurate simulation of the packaging forming process. Packag Technol Sci 2018;31(8):557–66.

[9] Xiong H, Guzman Maldonado E, Hamila N, Boisse P. A prismatic solid-shell finite element based on a DKT approach with efficient calculation of through the thickness deformation. Finite Elements in Analysis and Design 2018;151:18–33.

[10] Schwarze M, Reese S. A reduced integration solid-shell finite element based on the EAS and the ANS concept-Large deformation problems. Int. J. Numer. Meth. Engng. 2011;85(3):289–329.

[11] Schwarze M, Reese S. A reduced integration solid-shell finite element based on the EAS and the ANS concept-Geometrically linear problems. Int. J. Numer. Meth. Engng. 2009;80(10):1322–55.

[12] Pagani M, Reese S, Perego U. Computationally efficient explicit nonlinear analyses using reduced integration-based solid-shell finite elements. Computer Methods In Applied Mechanics And Engineering 2014;268:141–59.

[13] Reese S, Barfusz O, Schwarze M, Simon J-W. Solid-shell formulations based on reduced integration—investigations of anisotropic material behaviour, large deformation problems and stability. 11th International Conference "Shell Structures: Theory and Applications" (11th SSTA) 2017:31–9.

[14] Jože K. Multi-language and Multi-environment Generation of Nonlinear Finite Element Codes. Engineering with Computers 2002;18(4):312–27.

[15] Simo JC, Armero F. Geometrically non-linear enhanced strain mixed methods and the method of incompatible modes. Int. J. Numer. Meth. Engng. 1992;33(7):1413–49.

[16] Betsch P, Stein E. An assumed strain approach avoiding artificial thickness straining for a non-linear 4-node shell element. Commun. Numer. Meth. Engng. 1995;11(11):899–909.

[17] Bathe K-J, Dvorkin EN. A formulation of general shell elements-the use of mixed interpolation of tensorial components. International Journal for Numerical Methods in Engineering 1986;22:697–722.

[18] Puso MA. A highly efficient enhanced assumed strain physically stabilized hexahedral element. Int. J. Numer. Meth. Engng. 2000;49(8):1029–64.

[19] Boisse P, Colmars J, Hamila N, Naouar N, Steer Q. Bending and wrinkling of composite fiber preforms and prepregs. A review and new developments in the draping simulations. Composites Part B: Engineering 2018;141:234–49.

[20] Dörr D, Schirmaier FJ, Henning F, Kärger L. A viscoelastic approach for modeling bending behavior in finite element forming simulation of continuously fiber reinforced composites. Composites Part A: Applied Science and Manufacturing 2017;94:113–23.